Site-selective optical spectroscopy and upconversion mechanisms of the laser material $BaLu_2F_8:Er^{3+}$

Oliver S. Wenger, Daniel R. Gamelin, and Hans U. Güdel
Departement für Chemie und Biochemie, Universität Bern, Freiestrasse 3, CH-3000 Bern 9, Switzerland

A. V. Butashin and Alexander A. Kaminskii
Institute of Crystallography, Russian Academy of Sciences, Leninskii prospekt 59, 117333 Moscow, Russia
(Received 28 December 1998)

Crystals of $BaLu_2F_8$ doped with Er^{3+} 1.0 and 4.5 % were studied by high-resolution optical absorption, luminescence, and excitation spectroscopy in the temperature range 10–300 K with particular focus on the role of the two crystallographically different sites for the dopant ions in this host, referred to here as Er^{3+} ''*A*'' and ''*B*.'' Efficient green upconversion luminescence was observed at all temperatures between 10 and 300 K under both excitation into $^4I_{11/2}$ around 980 nm and into $^4I_{9/2}$ around 800 nm. For both excitation wavelengths excited state absorption (ESA) and energy transfer upconversion (ETU) were found to be active and could, in the case of $^4I_{11/2}$ excitation, be identified on the basis of time-resolved measurements. At 10 K, the $^4I_{11/2}$ and the $^4I_{9/2}$ excited states shows completely different behavior: whereas with $^4I_{9/2}$ excitation the Er^{3+} ''*A*'' and ''*B*'' sites act independently of each other, a directional Er^{3+} ''*B*''→''*A*'' energy transfer is observed upon $^4I_{11/2}$ excitation, leading to predominantly Er^{3+} ''*A*'' ETU luminescence. In contrast, upconversion luminescence excited via the $^4I_{11/2}$-ESA mechanism mainly occurs from Er^{3+} site ''*B*.'' Measured oscillator strengths of the observed f-f transitions are modeled using a Judd-Ofelt calculation, from which relevant ESA oscillator strengths are estimated. [S0163-1829(99)02028-7]

I. INTRODUCTION

Recently, there has been enormous interest among laser physicists and materials researchers in the development of visible and UV solid state phosphors or lasers which can be pumped by cheap diode lasers in the near IR. Upconversion, i.e., photoexcitation followed by luminescence at a shorter wavelength, is a common phenomenon among lanthanide doped compounds, and such compounds are therefore being actively investigated for potential materials applications.[1,2] Er^{3+} doped fluoride materials such as $LaF_3:Er^{3+}$, $LiYF_4:Er^{3+}$, and $BaY_2F_8:Er^{3+}$ are especially efficient upconverters.[3–5] This is due to the energy level scheme of Er^{3+} (Fig. 1) which is very favorable for serial addition of multiple isoenergetic photons. In contrast to low-phonon materials such as Ba_2YCl_7, $Cs_3Lu_2Br_9$, or $RbGd_2Br_7$, the number of excited states available for upconversion and luminescence processes is very limited in fluorides due to rather efficient multiphonon relaxation.[6–8] However, fluorides have the great advantage of being hard, stable in air and essentially insensitive to moisture. Thus, from a materials point of view, they are ideally suited for laser applications. Aside from upconversion studies, significant effort has been given to the development of new host materials. The title material, although known for quite a few years, has only recently become available in the form of single crystals with an optical quality sufficient for laser purposes.[9,10] In the present paper we investigate the orthorhombic high-temperature α modification which is metastable at room temperature. Recently, the suitability of this material for laser applications has been demonstrated by laser action at 300 K of the $^4I_{11/2}\rightarrow{}^4I_{13/2}$ transition around 2.8 μm.[11]

$BaLu_2F_8$ shows the typical properties of fluoride lattices mentioned above. In contrast with established fluoride laser hosts such as $LiYF_4:Er^{3+}$ or $BaY_2F_8:Er^{3+}$; however, Er^{3+} ions doped into the orthorhombic $BaLu_2F_8$ crystals (space group Pnma) may occupy one of two crystallographically inequivalent Lu^{3+} sites.[12] The structural properties of these two sites, in which the Er^{3+} ions are eightfold coordinated by F with C_1 site symmetry, are depicted in Fig. 1. The primary structural difference is given by the distances between the Lu and the F atoms: although the average Lu-F bond length is almost the same for both sites, these distances vary only up to 0.1 Å in site ''*A*,'' whereas in site ''*B*'' the maximum and minimum Lu-F bond lengths differ by 0.4 Å. The LuF_8 polyhedron of site ''*A*'' approaches more closely the spherical limit than site ''*B*.''

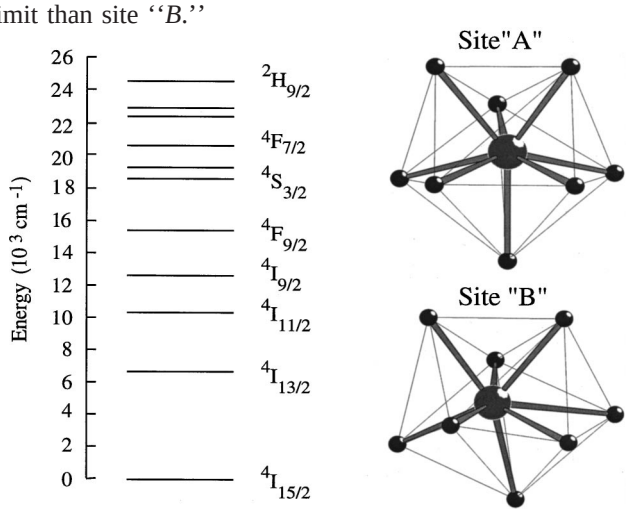

FIG. 1. Energy level scheme of Er^{3+} and the two crystallographically different LuF_8 polyhedra in $BaLu_2F_8$.

In this study we report on the NIR to VIS upconversion processes in α-$BaLu_2F_8$:Er^{3+}; we compare with the corresponding processes in the established upconversion laser materials $LiYF_4$:Er^{3+} and BaY_2F_8:Er^{3+}.[13,14] Because the presence of two dopant sites may introduce significant photophysical processes not present in the latter, we have given particular attention to the role of two different rare earth sites in the observed upconversion processes. These studies suggest that this system is a candidate for upconversion laser applications, and the spectroscopic and calculational results presented here provide a basis for the implementation of this material in upconversion laser experiments.

II. EXPERIMENT

A. Synthesis

Orthorhombic $BaLu_2F_8$ crystals doped with x% Er^{3+} ($x = 1.0, 4.5$) were synthesized by the Bridgman-Stockbarger technique in a HF atmosphere.[10,14] BaF_2, LuF_3, and ErF_3 were used as starting materials. Crystals of good optical quality were obtained up to 10 mm in diameter and 40 mm in length.

B. Spectroscopy

All spectra were measured unpolarized with a random crystal orientation. Sample cooling was achieved by a closed-cycle cryostat (Air Products Displex) for absorption measurements and with a He-flow technique for the emission experiments. Absorption spectra were measured on a Cary 5e (Varian) spectrometer. Continuous-wave luminescence and excitation measurements were performed using a Ti:sapphire laser (Schwartz Electro Optics), pumped by an argon laser (Spectra Physics 2045) in all-lines mode. Wavelength control was achieved by an inchworm driven (Burleigh PZ 501) birefringent filter. The sample luminescence was dispersed by a 0.85-m double monochromator (Spex 1402) using 500-nm blazed 1200 grooves/mm gratings and detected by a cooled photomultiplier (RCA 31034 or Hamamatsu C2761) using a photon counting system (Stanford Research SR400).

For pulsed luminescence experiments at the $^4I_{11/2}$ excitation energy around 10300 cm^{-1} the output of a frequency-doubled Nd^{3+}:YAG laser (Quanta Ray DCR-3, 10 Hz/20 Hz) pumped dye laser (Lambda Physik FL 3002, Pyridin 1 in methanol) was Raman shifted (Quanta Ray RS-1, H_2 340 psi). For direct $^4S_{3/2}$ excitation around 18 450 cm^{-1} the same setup was used but the output of the Raman shifter was anti-Stokes shifted. For direct $^4F_{9/2}$ excitation around 15 300 cm^{-1} the dye laser was used directly. The sample luminescence was dispersed by a 0.75-m single monochromator (Spex 1702) using 750-nm blazed 600 grooves/mm gratings and detected as described above. For time-resolved measurements a multichannel scaler (Stanford Research SR430) was used.

For spectroscopic comparison with the title compound, a $LiYF_4$:1% Er^{3+} crystal was used for absorption and emission experiments.

TABLE I. Comparison of experimental and calculated oscillator strengths obtained using the Judd-Ofelt model with the Slater integrals: $F_{(2)}=429.575$ cm^{-1}, $F_{(4)}=65.012$ cm^{-1}, $F_{(6)}=7.136$ cm^{-1}, and spin-orbit coupling constant $\xi=2383$ cm^{-1}. The multiplets used for the least-squares fit are indicated in boldface. The following intensity fit parameters were obtained: $\Omega_{(2)}=1.518\times10^{-20}$ cm^2, $\Omega_{(4)}=9.251\times10^{-21}$ cm^2, and $\Omega_{(6)}=1.133\times10^{-20}$ cm^2.

Transition	f_{obs} (10^{-6})	f_{calc} (10^{-6})	f_{calc}/f_{obs}
$^4I_{15/2}\rightarrow$ **$^4I_{13/2}$**	2.052	1.640	0.80
$^4I_{15/2}\rightarrow$ **$^4I_{11/2}$**	0.530	0.498	0.94
$^4I_{15/2}\rightarrow$ **$^4I_{9/2}$**	0.225	0.235	1.04
$^4I_{15/2}\rightarrow$ **$^4F_{9/2}$**	1.766	1.489	0.84
$^4I_{15/2}\rightarrow$ **$^4S_{3/2}$**	0.408	0.444	1.09
$^4I_{15/2}\rightarrow$ **$^2H_{11/2}$**	2.877	2.904	1.01
$^4I_{15/2}\rightarrow$ **$^4F_{7/2}$**	1.501	1.694	1.13
$^4I_{15/2}\rightarrow {}^4F_{5/2}/{}^4F_{3/2}$	0.686	0.876	1.28
$^4I_{15/2}\rightarrow {}^2H_{9/2}$	0.545	0.668	1.23
$^4I_{15/2}\rightarrow$ **$^4G_{11/2}$**	5.243	5.250	1.00
$^4I_{15/2}\rightarrow {}^2G_{9/2}/{}^2G_{7/2}$	1.878	1.737	0.92
$^4I_{15/2}\rightarrow {}^2P_{3/2}$	0.050	0.060	1.20
$^4I_{9/2}\rightarrow {}^2H_{9/2}$		13.337	

III. RESULTS

Absorption spectra were measured at various temperatures between 10 and 300 K. They consist of sharp and relatively weak lines, characteristic of f-f transitions. The assignment of the multiplets is straightforward from a comparison with the literature.[15] The oscillator strengths extracted from the room-temperature absorption spectrum are given in Table I, together with the corresponding calculated term to term oscillator strengths obtained using the Judd-Ofelt model; see Sec. IV A.[16,17]

In Table II the lifetimes of some relevant excited states extracted from time-dependent luminescence experiments are collected. They are given for $BaLu_2F_8$:Er^{3+} at 10 and 300 K for 1% Er^{3+} and at 10 K for 4.5% Er^{3+}, respectively.

Figure 2 shows the absorption spectrum of $BaLu_2F_8$:1% Er^{3+} in the $^4I_{9/2}$ region at 10 K (upper trace) and excitation spectra of the same sample monitoring the 10 K $^4I_{9/2}\rightarrow{}^4I_{15/2}$ luminescence at 12 378 and 12 366 cm^{-1} (middle and lower trace), respectively. In absorption, 9 Stark levels are detected. This number reveals the existence of two crystallographically different sites for the Er^{3+} dopant ions in

TABLE II. Lifetimes τ of some relevant excited states in $BaLu_2F_8$:1% Er^{3+} (10 and 300 K) and $BaLu_2F_8$:4.5% Er^{3+} (10 K). The lifetimes were measured after direct excitation of the respective excited states. Calculated data were obtained using the Judd-Ofelt model.

	$BaLu_2F_8$:1% Er^{3+}		$BaLu_2F_8$:4.5% Er^{3+}	Calculated
	τ (ms)	τ (ms)	τ (ms)	τ (ms)
Multiplet	$T=10$ K	$T=300$ K	$T=10$ K	
$^4I_{11/2}$	12.514	6.646	10.454	6.671
$^4F_{9/2}$	0.428	0.280	0.420	1.001
$^4S_{3/2}$	0.598	0.400	0.570	0.618

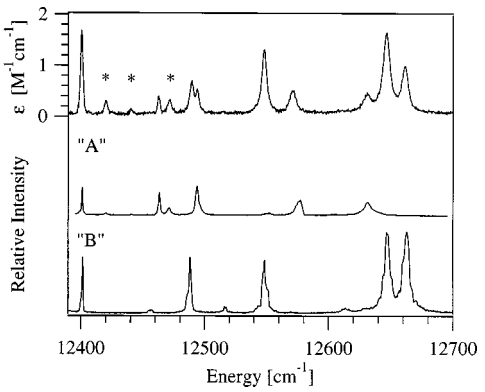

FIG. 2. Upper trace: $^4I_{15/2} \rightarrow {}^4I_{9/2}$ absorption spectrum of $BaLu_2F_8$:1% Er^{3+} at 10 K. The asterisks (*) indicate hot bands. Middle and lower trace: 10 K excitation spectra of the same sample with detection of luminescence at 12 378 and 12 366 cm^{-1}, respectively.

$BaLu_2F_8$. The individual ''*A*'' and ''*B*'' spectra can be obtained by using site-selective excitation spectroscopy, yielding the middle and bottom traces in Fig. 2, respectively. Both excitation spectra show the expected number of 5 $^4I_{9/2}$ Stark level excitations.

Figure 3 shows a comparison of high-resolution $^4I_{9/2} \rightarrow {}^4I_{15/2}$ luminescence spectra of $BaLu_2F_8$:1% Er^{3+} at 10 K for three different excitation energies. The upper spectrum was excited at 12 400 (sites ''*A*'' and ''*B*''), the middle at 12 631 (site ''*A*'') and the lower at 12 661 cm^{-1} (site ''*B*''), respectively. In each of the latter two spectra 8 peaks are observed as indicated by the brackets and as expected for the $^4I_{15/2}$ ground state. The upper spectrum is essentially a superposition of the two lower spectra.

In Figure 4 the 10-K absorption spectrum of $BaLu_2F_8$:1% Er^{3+} in the $^4I_{11/2}$ region is presented together with two excitation spectra of the same sample detecting the 10-K $^4I_{11/2} \rightarrow {}^4I_{15/2}$ luminescence at 10 191 (middle trace, sites ''*A*''+''*B*'') and at 10 187 cm^{-1} (bottom trace, site ''*B*''), respectively, as indicated by the asterisks in Fig. 5. Again the absorption spectrum is a superposition of sites ''*A*'' and ''*B*.'' From a comparison of the excitation spectra the pure ''*A*'' and ''*B*'' spectra can be identified, as emphasized in

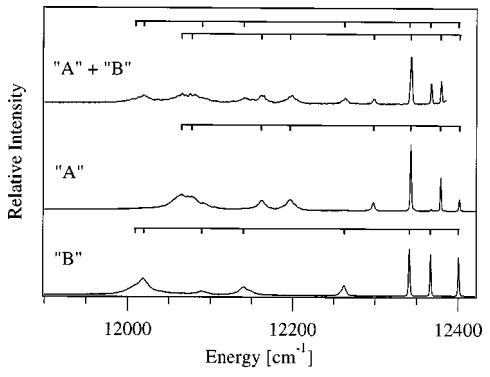

FIG. 3. 10 K luminescence spectra of $BaLu_2F_8$:1% Er^{3+} excited into $^4I_{9/2}$ at 12 400, 12 631, and 12 661 cm^{-1}, from top to bottom, respectively. The brackets indicate the Stark splittings of the $^4I_{15/2}$ ground state for the two sites ''*A*'' and ''*B*,'' respectively.

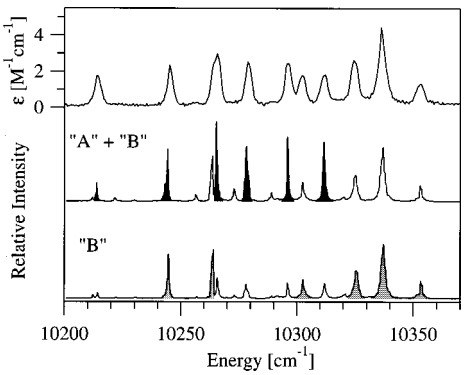

FIG. 4. The upper trace shows the $^4I_{15/2} \rightarrow {}^4I_{11/2}$ absorption spectrum of $BaLu_2F_8$:1% Er^{3+} at 10 K. The middle and the lower trace are 10 K excitation spectra detecting at 10 191 and 10 187 cm^{-1}, respectively, as indicated by the asterisks (*) in Fig. 5. The shaded areas indicate the $^4I_{11/2}$ Stark levels belonging to sites ''*A*'' and ''*B*,'' respectively.

black in Fig. 4. Both spectra consist of six Stark level excitations, as expected for $^4I_{11/2}$.

The high-energy part of the 10-K high-resolution $^4I_{11/2} \rightarrow {}^4I_{15/2}$ luminescence spectra excited at two different energies are presented in Fig. 5. The excitation energies were 10 312 and 10 336 cm^{-1} for the upper and the lower spectrum, respectively. In the upper spectrum the same $^4I_{15/2}$ Stark level splitting pattern as in the middle spectrum of Fig. 3 is identified, i.e., site ''*A*.'' The lower spectrum of Fig. 5 contains both ''*A*'' and ''*B*'' emission lines. We also investigated the temperature dependence of these luminescence spectra: above 50 K they essentially look the same (data not shown).

From the Figs. 2–5 the Stark level energies of the $^4I_{15/2}$, $^4I_{11/2}$, and $^4I_{9/2}$ multiplets were extracted and assigned to the two crystallographically different Er^{3+} sites (see Sec. IV B). The results are summarized in Table III.

Figure 6 shows the temporal behavior of the $^4I_{11/2} \rightarrow {}^4I_{15/2}$ luminescence of $BaLu_2F_8$:1% Er^{3+} at 10 K after a short (<10 ns) excitation pulse. Two different excitation energies were used: 10 214 (left) and 10 326 cm^{-1} (right),

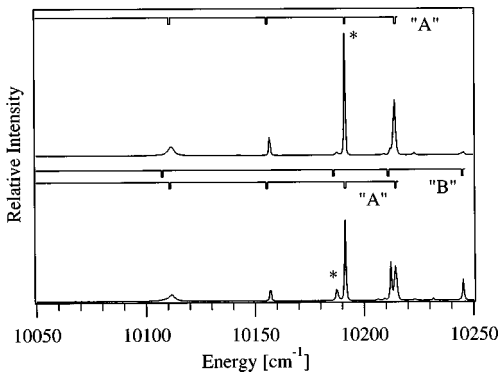

FIG. 5. 10 K luminescence observed after excitation into $^4I_{11/2}$ at 10 312 cm^{-1} (top) and 10 336 cm^{-1} (bottom). The brackets indicate the Stark splittings of the $^4I_{15/2}$ ground state for sites ''*A*'' and ''*B*,'' respectively. The asterisks (*) indicate the luminescence lines detected in Fig. 4.

TABLE III. Relevant energy levels in $BaLu_2F_8:Er^{3+}$ extracted from high-resolution absorption, luminescence, and excitation spectra. Energies are given in cm^{-1} relative to the lowest energy Stark level. ''*A*'' and ''*B*'' correspond to the two crystallographically different rare earth sites; see Fig. 1.

		''*A*''	''*B*''			''*A*''	''*B*''
$^4I_{15/2}$	(1)	0	0		(4)	10 279	10 326
	(2)	23	33		(5)	10 296	10 336
	(3)	58	58		(6)	10 312	10 353
	(4)	103	137				
	(5)	204	259	$^4I_{9/2}$	(1)	12 400	12 400
	(6)	239	310		(2)	12 462	12 489
	(7)	324	382		(3)	12 494	12 548
	(8)	336	391		(4)	12 571	12 647
					(5)	12 632	12 662
$^4I_{11/2}$	(1)	10 214	10 245				
	(2)	10 245	10 264	$^4S_{3/2}$	(1)	18 415	18 448
	(3)	10 267	10 302		(2)	18 478	18 502

respectively, with detection at 10 191 cm^{-1} for both. The left curve exhibits a simple exponential decay whereas the right curve shows a rise with a rate constant of 830 s^{-1} and a decay. From the semilogarithmic plots in the insets we see that both curves have the same single exponential decay behavior with a rate constant of 80 s^{-1}.

Figure 7 shows a comparison of upconversion luminescence spectra of $BaLu_2F_8$:1% Er^{3+} at 10 K for excitation into $^4I_{11/2}$ (top) and into $^4I_{9/2}$ (bottom) excited states, respectively. They are scaled to an equal integrated intensity of the $^4S_{3/2}\rightarrow{}^4I_{15/2}$ transition, which dominates both spectra. After $^4I_{9/2}$ excitation some weak $^2H_{9/2}\rightarrow{}^4I_{15/2}$ upconversion luminescence is observed. The $^4F_{9/2}\rightarrow{}^4I_{15/2}$ upconversion luminescence is relatively more intense after excitation into $^4I_{9/2}$.

In the upper part of Fig. 8 the 10-K absorption spectrum of $BaLu_2F_8$:1% Er^{3+} in the $^4S_{3/2}$ region is presented. The cold peaks are indicated by the upper brackets. The occurrence of two pairs of lines is due to the two Er^{3+} sites ''*A*'' and ''*B*,'' respectively. The lower part of Fig. 8 shows the high-resolution $^4S_{3/2}\rightarrow{}^4I_{15/2}$ upconversion luminescence of the same sample at 10 K after excitation into $^4I_{11/2}$ at 10 245 cm^{-1}, corresponding to site ''*B*;'' see Table III. The upconversion luminescence spectrum is a superposition of site ''*A*'' and ''*B*'' spectra with an approximative ratio of 5:1.

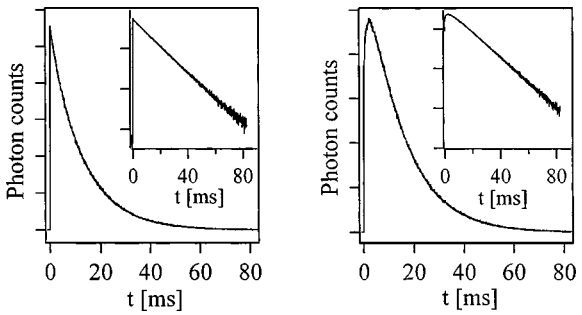

FIG. 6. Temporal behavior of $^4I_{11/2}$ luminescence of $BaLu_2F_8$:1% Er^{3+} at 10 K after a short (<10 ns) excitation pulse. Excitation energies were 10 214 cm^{-1} (site ''*A*'') and 10 326 cm^{-1} (site ''*B*''), detection was at 10 191 cm^{-1} (site ''*A*''). The insets show the same data in semilogarithmic representation.

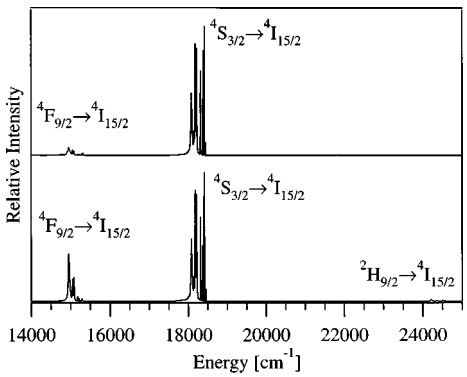

FIG. 7. Overview NIR→VIS upconversion spectra of $BaLu_2F_8$:1% Er^{3+} at 10 K after excitation into $^4I_{11/2}$ (upper trace) and $^4I_{9/2}$ (lower trace). The two spectra are normalized to an equal integrated intensity of the $^4S_{3/2}\rightarrow{}^4I_{15/2}$ transition.

Figure 9 shows temperature-dependent excitation spectra of $BaLu_2F_8$:1% Er^{3+} in the $^4I_{11/2}$ region, obtained while detecting the upconverted $^4S_{3/2}\rightarrow{}^4I_{15/2}$ transition at 18 448 cm^{-1} (site ''*B*''). The bottom trace is the $^4I_{15/2}\rightarrow{}^4I_{11/2}$ absorption spectrum of the same sample at 10 K. With the exception of the shaded peak centered at 10 326 cm^{-1}, all excitation peaks increase upon heating the sample from 10 to 30 K.

In Figure 10 we report the time evolution of the upconverted $^4S_{3/2}\rightarrow{}^4I_{15/2}$ luminescence of $BaLu_2F_8$:1% Er^{3+} detected at 18 415 cm^{-1} at 10 K after a short (<10 ns) excitation pulse. Two different excitation energies on site ''*B*'' within the $^4I_{11/2}$ multiplet were used: 10 326 cm^{-1} (left) and 10 245 cm^{-1} (right). Whereas the left curve shows an immediate decay with a dominant rate constant of 1405 s^{-1}, the right curve shows a slow rise after the excitation pulse, followed by a decay. The spike at $t=0$ is due to stray laser light. The insets show the same data in a semilogarithmic representation.

Figure 11 compares upconversion excitation spectra of

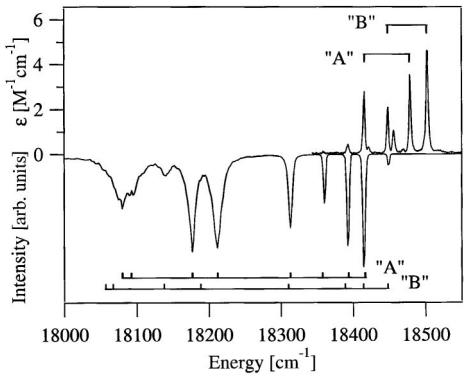

FIG. 8. The lower trace shows high-resolution $^4S_{3/2}\rightarrow{}^4I_{15/2}$ upconversion luminescence of $BaLu_2F_8$:1% Er^{3+} at 10 K. Excitation occured at 10 245 cm^{-1} into a $^4I_{15/2}\rightarrow{}^4I_{11/2}$ ground state absorption. The lower brackets indicate the Stark splittings of the ground state for the two sites ''*A*'' and ''*B*,'' respectively. The upper trace is a $^4I_{15/2}\rightarrow{}^4S_{3/2}$ absorption spectrum at 10 K. The upper brackets indicate $^4S_{3/2}$ levels belonging to sites ''*A*'' and ''*B*,'' respectively.

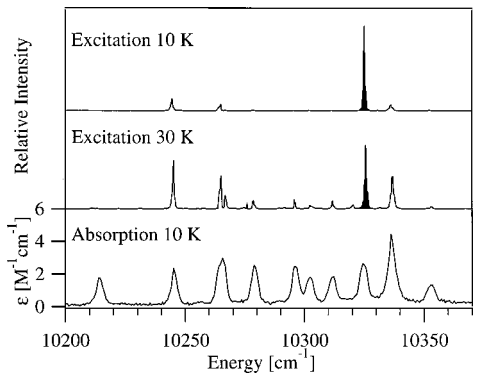

FIG. 9. Temperature dependence of the excitation spectrum, detecting the upconverted $^4S_{3/2}\rightarrow{}^4I_{15/2}$ luminescence of $BaLu_2F_8$:1% Er^{3+} at 18 448 cm^{-1} (site ''*B*''). The shaded area indicates a $^4I_{11/2}\rightarrow{}^4F_{7/2}$ excited state absorption process. The bottom trace is the $^4I_{15/2}\rightarrow{}^4I_{11/2}$ absorption spectrum at 10 K.

$BaLu_2F_8$:1% Er^{3+} in the $^4I_{9/2}$ region with the corresponding $^4I_{15/2}\rightarrow{}^4I_{9/2}$ absorption spectra at 10 and 300 K. For the excitation spectra the $^4S_{3/2}\rightarrow{}^4I_{15/2}$ upconversion luminescence was monitored at 18 415 cm^{-1}. At 10 K the upconversion excitation spectrum and the absorption spectrum are very similar. At 300 K the excitation spectrum differs significantly from absorption below 12 390 cm^{-1} (shaded area). This is clearly due to a thermally activated process.

IV. DISCUSSION

A. Absorption intensities and excited state lifetimes: a Judd-Ofelt analysis

The oscillator strengths of term to term transitions within the *f*-electron configuration were calculated using Judd-Ofelt theory based on the unpolarized room-temperature absorption spectrum.[16,17] The atomic parameters for $BaLu_2F_8$:Er^{3+} were estimated from those of LaF_3:Er^{3+} as $F_{(2)}=429.575\,cm^{-1}$, $F_{(4)}=65.012\,cm^{-1}$, $F_{(6)}=7.136\,cm^{-1}$, and $\xi=2383\,cm^{-1}$.[18] The differences between the two sites for the Er^{3+} ions are neglected in this approach. Table I shows that the 12 experimental values are very well reproduced by fitting the three Judd-Ofelt parameters $\Omega_{(2)}$, $\Omega_{(4)}$, and $\Omega_{(6)}$.

On the basis of the Judd-Ofelt parameters deduced from the absorption intensities we calculated the radiative lifetimes of the relevant excited states. A comparison with measured lifetimes is given in Table II. For $^4S_{3/2}$ the agreement is very good, thus indicating that relaxation from this multiplet is almost purely radiative. The observed decrease of $\tau(^4S_{3/2})$ from 598 to 400 μs between 10 and 300 K is attributed to the thermally activated cross relaxations $^2H_{11/2}+{}^4I_{15/2}\rightarrow{}^4I_{9/2}+{}^4I_{13/2}$ and $^2H_{11/2}+{}^4I_{15/2}\rightarrow{}^4I_{13/2}+{}^4I_{9/2}$ due to the increased $^2H_{11/2}$ population at 300 K. A similar behavior was observed in YF_3:Er^{3+}.[19] The calculated radiative lifetimes for the $^4F_{9/2}$ and the $^4I_{11/2}$ multiplets differ from the measured low-temperature values of $BaLu_2F_8$:1% Er^{3+} by factors of about 2. This is within the accuracy of Judd-Ofelt theory, especially when the initial multiplet is not in thermal equilibrium.

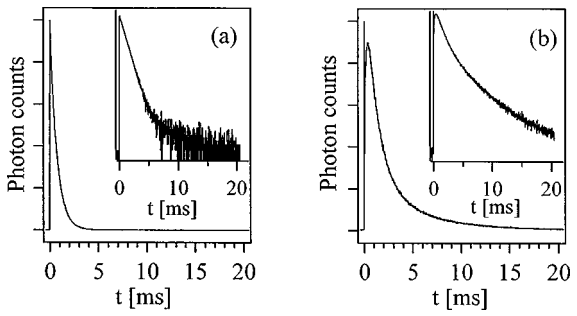

FIG. 10. $^4S_{3/2}\rightarrow{}^4I_{15/2}$ upconversion luminescence transients of $BaLu_2F_8$:1% Er^{3+} at 10 K detected at 18 415 cm^{-1} (site ''*A*'' + ''*B*'') after $^4I_{11/2}$ excitation at (a) 10 326 cm^{-1} (site ''*B*'') and at (b) 10 245 cm^{-1} (site ''*A*'' + ''*B*''). The excitation pulse has a width of 8 ns and occurs at $t=0$. The insets show the same data in a semilogarithmic plot.

When increasing the Er^{3+} dopant concentration from 1% to 4.5% the $^4S_{3/2}$, $^4F_{9/2}$, $^4I_{11/2}$ lifetimes are reduced by 5%, 2%, and 16%, respectively. This indicates that concentration quenching is still relatively weak in the 4.5% Er^{3+} doped crystal. In BaY_2F_8:Er^{3+} it was observed that the rate constant of the energy transfer upconversion step $^4I_{11/2}+{}^4I_{11/2}\rightarrow{}^4I_{15/2}+{}^4F_{7/2}$ increases by a factor of 3 when increasing the dopant concentration from 1% to 5%.[20] A similar effect is believed to contribute to the reduction of the $^4I_{11/2}$ lifetime in the $BaLu_2F_8$:4.5% Er^{3+} crystal compared to the 1% Er^{3+} sample. Finally, the $^4I_{11/2}$ lifetime is observed to be strongly temperature dependent, and this is attributed to a thermally activated intersite energy transfer process as described in Sec. IV C.

B. Spectroscopic deconvolution of the two Er^{3+} sites

In the free Er^{3+} ion the $|SLJ\rangle$ terms are $(2J+1)$-fold degenerate. If the ion is introduced into a crystal, it experiences the crystal field. This electrostatic field removes part of the $|SLJ\rangle$ degeneracy by splitting them into several Kramers doublet Stark levels. Since there exist two crystallographically distinct sites for the Er^{3+} dopant ions in $BaLu_2F_8$, each with

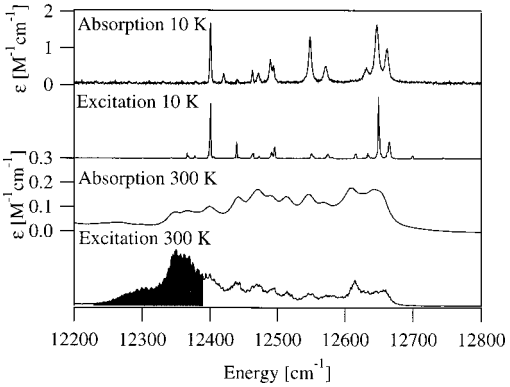

FIG. 11. Comparison of $^4I_{9/2}$ excitation spectra, detecting the upconverted $^4S_{3/2}\rightarrow{}^4I_{15/2}$ luminescence at 18 415 cm^{-1}, with the corresponding absorption spectra at 10 and 300 K. The shaded area indicates a $^4I_{9/2}\rightarrow{}^2H_{9/2}$ excited state absorption process.

point symmetry C_1, $2J+1$ Stark levels are expected for each multiplet, $(2J+1)/2$ per Er^{3+} site.

The $^4I_{9/2}$ absorption spectrum (Fig. 2, top) shows nine Stark levels. Excitation into the origin leads to a luminescence spectrum (Fig. 3, top) which clearly contains more than eight lines, thus indicating that both Er^{3+} sites luminesce under these conditions. Excitation scans of its two highest energy features provide two completely different spectra (Fig. 2, middle, bottom), each of them consisting of five cold excitation peaks. The superposition of the two excitation spectra perfectly reproduces the absorption spectrum. Thus, it is concluded that each of the former shows the five $^4I_{9/2}$ Stark levels of a single Er^{3+} site. This is confirmed by the luminescence spectra obtained after excitation into the respective Stark levels (Fig. 3, middle, bottom). In each spectrum eight different $^4I_{15/2}$ ground state Stark levels are observed, as expected for a single Er^{3+} site. The $^4I_{15/2}-{}^4I_{9/2}$ origins of both sites coincide at 12 400 cm^{-1}. This accounts for the occurence of nine (instead of ten) Stark levels in absorption and for the multitude of lines observed in luminescence after excitation at this energy (Fig. 3, top). Thus, using excitation spectroscopy we are able to deconvolute the $^4I_{9/2}$ absorption spectrum and assign all $^4I_{9/2}$ Stark levels to the two crystallographically different Er^{3+} sites. After excitation into the respective Stark levels we obtain all $^4I_{15/2}$ ground state Stark level energies for both Er^{3+} sites by luminescence spectroscopy. This is an important result that allows the luminescence properties of other excited states to be investigated in more detail.

As shown in Table III, the Stark splittings of the multiplets of site ''*B*'' are always greater than those of site ''*A*'' (with the exception of $^4S_{3/2}$). We therefore associate the Er^{3+} site ''*B*'' with the more distorted ErF_8 polyhedron in Fig. 1 since this is expected to show a stronger Stark effect than the less distorted site ''*A.*'' This assignment is in agreement with the lower oscillator strength observed in the site ''*A*'' excitation spectrum of $^4I_{9/2}$ (Fig. 2, middle) relative to the site ''*B*'' spectrum (Fig. 2, bottom), since the site ''*A*'' ErF_8 polyhedron is closer to spherical than site ''*B.*''

In contrast to $^4I_{9/2}$ it was not possible to obtain a clean $^4I_{11/2}$ excitation or luminescence spectrum for site ''*B.*'' As shown in Fig. 5 we observed either luminescence exclusively from site ''*A*'' or from both sites. This suggests that site ''*B*'' excitation always leads to partial energy transfer to site ''*A.*'' This is confirmed by time-resolved spectroscopy (Sec. IV C). Monitoring site ''*B*'' luminescence we identified the 6 site ''*B*'' Stark levels of $^4I_{11/2}$ (Fig. 4, bottom, shaded peaks). These six peaks also occur in the excitation spectrum of the site ''*A*'' luminescence (middle trace in Fig. 4), a clear indication that Er^{3+} ions on site ''*B*'' sensitize site ''*A*'' luminescence. The bottom trace of Fig. 4 is not a completely clean site ''*B*'' excitation spectrum. The presence of very weak site ''*A*'' lines indicates that ''*A*'' to ''*B*'' energy transfer also occurs, but at 10 K it is inefficient.

C. Energy transfer between the two Er^{3+} sites

After site ''*B*'' excitation the $^4I_{11/2}$ luminescence spectrum consists of approximately 75% site ''*A*'' luminescence (Fig. 5, bottom). The rate constant of this energy transfer process at 10 K is determined from the data in Fig. 6 to be

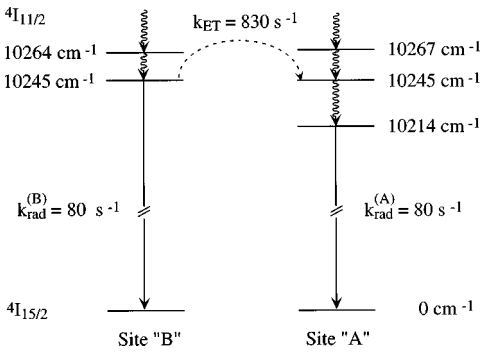

FIG. 12. Schematic representation of the energy transfer between the sites ''*B*'' and ''*A*'' in the $^4I_{11/2}$ state of $BaLu_2F_8$:1% Er^{3+} at 10 K. The $^4I_{11/2}$ Stark level energies are taken from Table III. The curly arrows represent multiphonon relaxation processes.

$k_{ET}=830\,s^{-1}$, which is an order of magnitude faster than the decay rate constant of $^4I_{11/2}$, which is $k_{rad}=80\,s^{-1}$ (Fig. 6). The order of magnitude difference between these two rates accounts for the high efficiency of the ''*B*''→''*A*'' energy transfer in this multiplet, and it reflects a good overlap of the donor emission with the acceptor absorption profile.[21] This overlap occurs at 10 245 cm^{-1} (Fig. 4), the lowest energy Stark level of $^4I_{11/2}$ for site ''*B.*'' At this energy there is a coincidence with the second $^4I_{11/2}$ Stark level of site ''*A*'' as shown in Fig. 12. Radiative decay of the ''*B*'' excitation and resonant ''*B*''→''*A*'' energy transfer thus compete. At low temperatures, ''*B*''→''*A*'' energy transfer is followed by rapid relaxation to the lowest Stark level of ''*A*'' at 10 214 cm^{-1}, from which emission occurs. At higher temperatures the 10 245 cm^{-1} level of site ''*A*'' is thermally populated and ''*A*''→''*B*'' energy transfer occurs. This is manifested in the temperature-dependence of the $^4I_{11/2}\rightarrow{}^4I_{15/2}$ luminescence spectra: above 50 K these spectra show increased site ''*B*'' luminescence and are independent of the initially excited Er^{3+} site. This behavior partly accounts for the observed decrease of the $^4I_{11/2}$ lifetime between 10 K and 300 K. The presence of such intersite energy transfer processes thus has important consequences for the excited state populations and the upconversion properties of this system (see Sec. IV D), and it is one of the distinguishing features of this crystal lattice when compared to established laser materials such as LaF_3 or $LiYF_4$ or BaY_2F_8.

Although a similar coincidence of Stark levels from both sites occurs in $^4I_{9/2}$ at 12 400 cm^{-1} (Fig. 2), no energy transfer is observed after $^4I_{9/2}$ excitation. Since this multiplet is only about 2000 cm^{-1} above $^4I_{11/2}$, its intrinsic lifetime is expected to be short due to efficient nonradiative multiphonon relaxation in the fluoride host lattice. For $LiYF_4$:1% Er^{3+} at 300 K a lifetime of 7 μs was reported.[22] Its corresponding decay rate is therefore ca. two orders of magnitude faster than the site ''*B*''→''*A*'' energy transfer rate determined for $^4I_{11/2}$. We conclude that in $^4I_{9/2}$ the energy transfer rate is not competitive with the multiphonon relaxation to $^4I_{11/2}$.

D. Upconversion mechanisms

The long lifetime of the $^4I_{11/2}$ excited state in $BaLu_2F_8$:Er^{3+} is favorable for upconversion processes in-

volving this multiplet after near IR excitation. As discussed in Sec. IV C, $^4I_{9/2}$ excitation also leads to $^4I_{11/2}$ population by fast multiphonon relaxation. Therefore, excitation of these two multiplets results in very similar upconversion luminescence spectra (Fig. 7). As usual for Er^{3+} doped fluoride host lattices, the upconversion luminescence spectrum is dominated by the green $^4S_{3/2}\rightarrow{}^4I_{15/2}$ transition. This is due to the small energetic separations between higher lying energy levels and $^4S_{3/2}$ (see Fig. 1) which leads to efficient multiphonon relaxation processes. In contrast, the energy gap below $^4S_{3/2}$ is large enough to keep the multiphonon relaxation rate small compared to the radiative rate. $^4I_{9/2}$ excitation leads to some additional weak $^2H_{9/2}\rightarrow{}^4I_{15/2}$ luminescence in the blue spectral region since in that case $^2H_{9/2}$ is populated via a two-photon process. Upconversion processes involving more than two photons are generally less efficient, thus $^2H_{9/2}$ is not significantly populated upon $^4I_{11/2}$ excitation. Changing the excitation from $^4I_{11/2}$ to $^4I_{9/2}$ increases the relative amount of yellow $^4F_{9/2}\rightarrow{}^4I_{15/2}$ upconversion luminescence. This is possibly due to the cross relaxations $^4I_{9/2}+{}^4S_{3/2}\rightarrow{}^4F_{9/2}+{}^4F_{9/2}$ and $^4I_{13/2}+{}^2H_{9/2}\rightarrow{}^4F_{9/2}+{}^4F_{9/2}$ which require nonzero $^4I_{9/2}$ and $^2H_{9/2}$ populations, respectively.[7]

In principle, upconversion can occur via two distinct processes, namely, by the radiative excited state absorption (ESA) or by nonradiative energy transfer upconversion (ETU) between two excited ions.[23,24] There are two possibilities to distinguish between these two processes: Upconversion luminescence excitation spectra and the time evolution of the upconversion luminescence after an excitation pulse.[7,25] For ETU the pathway by which the involved ions are excited into the intermediate state is unimportant. The subsequent ETU step can be phonon-assisted and requires no exact energy resonance between the intermediate and the upper state involved in the upconversion process. Therefore, an ETU excitation spectrum is very similar to the absorption spectrum of the intermediate state. On the other hand, the ESA upconversion process requires an exact resonance between the ground state absorption (GSA) and an excited state absorption. Therefore an ESA upconversion excitation spectrum resembles the product of the GSA and ESA spectra, and may differ dramatically from the GSA spectrum of the intermediate state. An unambiguous distinction between the two mechanisms can be performed by time-dependent measurements, i.e., probing the time evolution of the upconversion luminescence after an excitation pulse of a few nanoseconds width. For ESA upconversion both GSA and ESA steps have to occur within the duration of the laser pulse, resulting in an immediate decay of the upconversion luminescence intensity after excitation. The nonradiative ETU processes, on the other hand, can still proceed after the pulse, and this is observed as a rise in upconversion luminescence preceding its decay.

At 10 K the high-resolution spectra of the $^2H_{9/2}\rightarrow{}^4I_{15/2}$, $^4S_{3/2}\rightarrow{}^4I_{15/2}$ (Fig. 8), and $^4F_{9/2}\rightarrow{}^4I_{15/2}$ upconversion luminescences for both $^4I_{11/2}$ and $^4I_{9/2}$ excitation reflect the behavior of the intermediate $^4I_{11/2}$ state with respect to intersite energy transfer. Except for the excitation energy 10 326 cm^{-1} (Sec. IV D 2), all upconversion luminescence spectra are dominated by luminescence from site ''*A*,'' independent of the initially excited multiplet or site in the near IR. Although we also observed ''*B*''$\rightarrow$''*A*'' energy transfer in the $^4S_{3/2}$ multiplet, the intensity distribution between the two rare earth sites ''*A*'' and ''*B*'' in upconversion luminescence favors site ''*A*'' luminescence and is clearly determined by the energy transfer occurring in the intermediate $^4I_{11/2}$ state. This confirms the statement from Sec. IV C: most of the $^4I_{9/2}$ excited Er^{3+} ions rapidly relax into $^4I_{11/2}$ where the intersite energy transfer takes place.

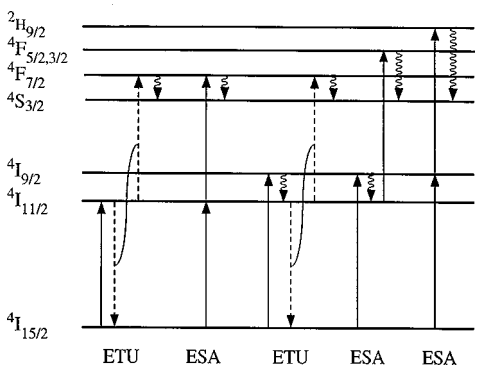

FIG. 13. Schematic representation of the observed upconversion processes in $BaLu_2F_8$: Er^{3+} after $^4I_{11/2}$ and $^4I_{9/2}$ excitation, respectively. Radiative and nonradiative processes are indicated by full and broken arrows, respectively. The curly arrows represent multiphonon relaxation processes.

1. ETU from the $^4I_{11/2}$ multiplet

Detecting site ''*B*'' upconversion luminescence at 18 448 cm^{-1} at 10 K, all intense excitation peaks in the $^4I_{11/2}$ region (Fig. 9, top) occur at energies that coincide with the $^4I_{15/2}\rightarrow{}^4I_{11/2}$ ground state absorption of site ''*B*,'' although their relative intensities differ from those in absorption. Since we are monitoring clean site ''*B*'' upconversion luminescence and since ''*A*''$\rightarrow$''*B*'' energy transfer in the intermediate $^4I_{11/2}$ state is very inefficient at 10 K, site ''*B*'' peaks dominate the excitation spectrum. The temperature-dependence shows that all the unshaded peaks increase when the temperature is elevated (Fig. 9, middle), suggesting that all of them are due to ETU: As we see from variable temperature absorption and luminescence spectra (data not shown), the spectral overlaps between donor emission and acceptor absorption profiles required for these energy transfer processes increase at elevated temperatures, and thus the energy transfer rate increases with increasing temperature. As discussed in Sec. IV C, ''*A*''$\rightarrow$''*B*'' energy transfer in the $^4I_{11/2}$ multiplet occurs at elevated temperatures, which explains the observed site ''*A*'' peaks in the 30 K upconversion luminescence excitation spectrum of Fig. 9. The ETU mechanism is confirmed by the time-dependent measurements (Fig. 10, right): the observed rise of the upconversion transient after pulsed excitation is the typical fingerprint for ETU processes. This ETU mechanism is schematically shown in Fig. 13 (first feature).

2. ESA from the $^4I_{11/2}$ multiplet

Although the majority of the peaks in the $^4I_{11/2}$ upconversion excitation spectrum of Fig. 9 can be attributed to ETU

mechanisms, significant ESA upconversion is also observed. At 10 K the most efficient upconversion process takes place after excitation into the shaded peak centered at 10 326 cm^{-1}. This is also true when monitoring site ''*A*'' luminescence. The upconversion transient observed after excitation at 10 326 cm^{-1} (Fig. 10, left), shows an immediate decay and thus reveals an ESA mechanism, as depicted schematically in Fig. 13 (second feature). From low-temperature absorption data we find that at this energy there is a coincidence of a $^4I_{15/2} \rightarrow {}^4I_{11/2}$ GSA with a $^4I_{11/2} \rightarrow {}^4F_{7/2}$. ESA. It is interesting to note that excitation at 10 326 cm^{-1} leads to the most intense site ''*B*'' upconversion luminescence, indicating that this mechanism takes place on Er^{3+} site ''*B*.'' Since ETU favors site ''*A*'' upconversion, we can therefore tune the ratio of site ''*A*:'' site ''*B*'' upconversion luminescence intensity by simply changing the excitation energy by a few wave numbers. From Fig. 9 we see that the ESA upconversion process becomes relatively less important with increasing temperature. ETU processes are taking over due to population of higher Stark levels both in the $^4I_{15/2}$ ground and $^4I_{11/2}$ intermediate state.

3. Upconversion from the $^4I_{9/2}$ multiplet

At very low temperatures, the upconversion excitation spectrum in the $^4I_{9/2}$ region (Fig. 11, upper half) is very similar to the corresponding absorption spectrum. As stated above, this is typical for ETU. Energy considerations lead to the same conclusion: at 10 K, twice the energy of the $^4I_{9/2}$ origin is already 43 cm^{-1} higher in energy than the highest Stark level of the upper $^2H_{9/2}$ multiplet. In addition, there is no evidence in the low-temperature excitation spectrum for a $^4I_{11/2} \rightarrow {}^4F_{5/2}/{}^4F_{3/2}$ excited state absorption. The main upconversion mechanism after $^4I_{9/2}$ excitation is thus ETU as depicted schematically in Fig. 13 (third feature): From the observed $^4I_{9/2}$ lifetime in $LiYF_4:Er^{3+}$ of 7 μs and the calculated radiative lifetime of $^4I_{9/2}$ of 6 ms we estimate that $^4I_{9/2} \rightarrow {}^4I_{11/2}$ multiphonon relaxation is three orders of magnitude more efficient than radiative decay.[22] $^4I_{9/2}$ excitation thus mainly leads to $^4I_{11/2}$ population. From there, the same ETU mechanism occurs as after direct $^4I_{11/2}$ excitation.

At 300 K, new intensity (shaded area) is observed in the upconversion excitation spectrum below 12 390 cm^{-1}, for which there is no corresponding feature in the 300 K absorption spectrum. $^4I_{15/2} \rightarrow {}^4I_{9/2}$ and $^4I_{15/2} \rightarrow {}^2H_{9/2}$ as well as $^4I_{15/2} \rightarrow {}^4I_{11/2}$ and $^4I_{15/2} \rightarrow {}^4F_{5/2}/{}^4F_{3/2}$ room-temperature absorption spectra show that a resonance of the $^4I_{15/2} \rightarrow {}^4I_{9/2}$ GSA with the $^4I_{11/2} \rightarrow {}^4F_{5/2}/{}^4F_{3/2}$ ESA as well as a resonance of the former with the $^4I_{9/2} \rightarrow {}^2H_{9/2}$ ESA is energetically possible below 12 390 cm^{-1} at this temperature. As stated above, $^4I_{9/2}$ excitation leads to a $^4I_{11/2}$:$^4I_{9/2}$ population ratio of approximately 1000:1. On the other hand, using the Judd-Ofelt model, we calculate a very high oscillator strength of $f = 13.337 \times 10^{-6}$ (Table II) for the $^4I_{9/2} \rightarrow {}^2H_{9/2}$ ESA which is an order of magnitude bigger than the calculated value for the $^4I_{11/2} \rightarrow {}^4F_{5/2}/{}^4F_{3/2}$ ESA oscillator strength ($f = 0.7 \times 10^{-6}$). We therefore conclude that, at room temperature, upconversion after $^4I_{9/2}$ excitation below 12 390 cm^{-1} takes place via the ESA mechanisms depicted in Fig. 13 (fourth and fifth feature), with the mechanism involving the $^4I_{11/2}$ intermediate state dominating by about two orders of magnitude.

V. CONCLUSIONS

We used absorption, luminescence, excitation and time-resolved spectroscopy to characterize the new laser material $BaLu_2F_8:Er^{3+}$. The presence of two crystallographically distinct sites in this host leads to unusual upconversion dynamics that involve not just excited state energy transfer between like sites but also between distinct sites. Using excitation spectroscopic techniques we were able to assign all Stark levels of the most important multiplets involved in upconversion processes to the two crystallographically different Er^{3+} sites. Both excited state absorption (ESA) and energy transfer upconversion (ETU) processes take place and can unambiguously be identified on the basis of their upconversion transients. ETU occurs at all temperatures between 10 and 300 K, irrespective of the initially excited site or multiplet in the near IR. ETU luminescence spectra are dominated by luminescence from Er^{3+} site ''*A*'' due to the rapid ''*B*'' $\rightarrow$ ''*A*'' energy transfer that occurs in the $^4I_{11/2}$ state, which is the most important intermediate state for ETU processes in this host. Depending on the exact excitation energy, ESA upconversion processes can be observed with excitation into the $^4I_{11/2}$ or the $^4I_{9/2}$ multiplets. $^4I_{11/2}$ ESA upconversion occurs on site ''*B*'' leading to a pronounced site ''*B*'' luminescence intensity. The temperature-dependence of the ESA mechanisms is opposite in the two multiplets: whereas $^4I_{11/2}$ ESA upconversion takes place only at very low temperatures, $^4I_{9/2}$ ESA upconversion only occurs close to room temperature.

As mentioned in the Introduction, the existence of two crystallographically distinct sites for the Er^{3+} dopant ions leads to the possibility of new upconversion processes not present in more established host lattices such as $LiYF_4:Er^{3+}$ or $BaY_2F_8:Er^{3+}$. In particular, the presence of two sites increases the density of states by a factor of 2 in this host, and presents the interesting possibility that this may increase upconversion efficiencies by making the energy match required for upconversion more likely to occur. A condition for that is an intense communication between the ions in the sites ''*A*'' and ''*B*.'' We have established that in $BaLu_2F_8$:1% Er^{3+} this intersite communication takes place in the $^4I_{11/2}$ and the $^4S_{3/2}$ excited states, even at 10 K. Although spectroscopically more difficult to resolve such two-site processes are expected to become more important at room temperature.

Regarding potential laser application, it is noted that the room-temperature $^4S_{3/2}$ lifetime of $BaLu_2F_8$:1% Er^{3+} (400 μs) is essentially the same as the one reported for $LiYF_4:Er^{3+}$, whereas the room-temperature lifetime of the intermediate $^4I_{11/2}$ multiplet is more than a factor of two longer in $BaLu_2F_8$:1% Er^{3+} (6.646 ms vs 2.9 ms).[22] For a given pump rate, this longer lifetime leads to a larger intermediate excited-state population N_1 in $BaLu_2F_8:Er^{3+}$ than in $LiYF_4:Er^{3+}$. The spectral overlap integrals of the room-temperature $^4I_{11/2} \rightarrow {}^4I_{15/2}$ emission and the $^4I_{11/2} \rightarrow {}^4F_{7/2}$ excited state absorption differ by less than 10% between $BaLu_2F_8:Er^{3+}$ and $LiYF_4:Er^{3+}$. From this and the comparable Er^{3+}-Er^{3+} distances in equally doped crystals, similar $^4I_{11/2} + {}^4I_{11/2} \rightarrow {}^4I_{15/2} + {}^4F_{7/2}$ ETU rate constants ω_{ETU} are es-

timated for both systems. Thus, for a given pump rate, the corresponding ETU rate, which is proportional to $\omega_{ETU}N_1^2$, is roughly four times larger in $BaLu_2F_8:Er^{3+}$ than in $LiYF_4:Er^{3+}$. Based on this observation, we consider $BaLu_2F_8:Er^{3+}$ to be a promising potential upconversion laser material for green $^4S_{3/2}\rightarrow{}^4I_{15/2}$ emission and one deserving further study in this regard.

ACKNOWLEDGMENTS

Financial support by the Swiss National Science Foundation is gratefully acknowledged. The Russian authors acknowledge also partial financial support from the Russian Foundation for Basic Research, as well as the State Scientific Programs ''Fundamental Metrology'' and ''Fundamental Spectroscopy.''

[1] W. Lenth and R. M. Macfarlane, Opt. Photonics News **3**, 8 (1992).
[2] E. Downing, L. Hesselink, J. Ralston, and R. Macfarlane, Science **273**, 1185 (1987).
[3] H. P. Jenssen, J. Phys. Colloq. **C7**, 427 (1987).
[4] G. J. Kintz, R. Allen, and L. Esterowitz, Appl. Phys. Lett. **50**, 1553 (1987).
[5] S. A. Pollack and D. B. Chang, Opt. Quantum Electron. **22**, S75 (1990).
[6] T. Riedener, P. Egger, J. Hulliger, and H. U. Güdel, Phys. Rev. B **56**, 1800 (1997).
[7] M. P. Hehlen, K. Krämer, and H. U. Güdel, Phys. Rev. B **49**, 12 475 (1994).
[8] T. Riedener, K. Krämer, and H. U. Güdel, Inorg. Chem. **34**, 2745 (1995).
[9] A. A. Kaminskii, A. V. Butashin, and S. N. Bagaev, Quantum Electron. **26**, 753 (1996).
[10] A. A. Kaminskii, A. V. Butashin, J. Hulliger, Ph. Egger, S. N. Bagayev, H. J. Eichler, J. Findeisen, B. Liu, U. Täuber, P. Peuser, and S. N. Sulyanov, J. Alloys Compd. **275-277**, 442 (1998).
[11] A. A. Kaminskii and A. V. Butashin, Phys. Status Solidi A **157**, K29 (1996).
[12] I. Sirota B. V. Bukvetskii, and V. I. Simonov, Krystallografiya **20**, 642 (1975) [Sov. Phys. Crystallogr. **20**, 393 (1975)].
[13] Brede, T. Danger, E. Heumann, G. Huber, and B. H. T. Chai, Appl. Phys. Lett. **63**, 729 (1993).
[14] R. A. McFarlane, J. Opt. Soc. Am. B **11**, 871 (1994).
[15] G. H. Dieke, *Spectra and Energy Levels of Rare Earth Ions in Crystals* (Wiley, New York, 1968).
[16] B. R. Judd, Phys. Rev. **127**, 750 (1962).
[17] G. S. Ofelt, J. Chem. Phys. **37**, 511 (1962).
[18] W. F. Krupke, Phys. Rev. **145**, 325 (1966).
[19] J. P. van der Ziel, F. W. Ostermayer, and L. G. Uitert, Phys. Rev. B **2**, 4432 (1970).
[20] D. S. Knowles and H. P. Jenssen, IEEE J. Quantum Electron. **28**, 1197 (1992).
[21] Th. Förster, Ann. Phys. (Leipzig) **2**, 55 (1948).
[22] J. Rubin, A. Brenier, R. Moncorgé, and C. Pedrini, J. Lumin. **36**, 39 (1986).
[23] F. E. Auzel, Proc. IEEE **61**, 758 (1973).
[24] J. C. Wright, Top. Appl. Phys. **15**, 239 (1976).
[25] M. P. Hehlen, G. Frei, and H. U. Güdel, Phys. Rev. B **50**, 16 264 (1994).